

## Analysis of self-written waveguides in photopolymers and photosensitive materials

Tanya M. Monro,<sup>1,2</sup> L. Poladian,<sup>2</sup> and C. Martijn de Sterke<sup>1,2</sup>

<sup>1</sup>*Department of Theoretical Physics, School of Physics, University of Sydney, New South Wales 2006, Australia*

<sup>2</sup>*Australian Photonics CRC, 101 National Innovation Centre, Australian Technology Park, Eveleigh, New South Wales 1430, Australia*

(Received 15 July 1997)

We develop a series expansion technique for analyzing the waveguides which can be self-written in photosensitive materials and photopolymers. Series expansions of the electric field amplitude and the refractive index distribution in the propagation distance are used to describe the primary eye, a feature that indicates that a waveguide is being formed in the material. We apply this technique to arbitrary incident beams and geometries, and we also take the material loss and saturation of the refractive index into account.

[S1063-651X(97)08412-2]

PACS number(s): 42.65.Sf, 78.20.Bh, 42.65.Tg, 42.70.Gi

### I. INTRODUCTION

Previous theoretical work [1,2] indicates that a channel waveguide can be self-written in a planar slab of photosensitive glass by a Gaussian beam at a wavelength at which the material is photosensitive. This occurs for both one- and two-photon photosensitivity models [2]. We have found that self-written waveguides also form in bulk photosensitive materials, where no waveguide is present initially.

Consider a Gaussian beam incident on a photosensitive material. Initially, the beam diffracts (as in Fig. 1 for a bulk material). The photosensitivity of the material causes the refractive index to increase, and it increases most where the intensity is highest. Hence the refractive index change is greatest on the axis of propagation of the beam, and so the beam is guided more strongly along this axis. We have shown that over time this effect leads to the formation of a channel waveguide in the glass. The structure of the resulting waveguide depends on the choice of input beam profile. Different choices of the incident beam shape allow the properties of the resulting waveguide to be tailored to suit the desired application.

Although self-writing in a photosensitive glass has yet to be demonstrated experimentally, other self-writing processes have been observed. For example, photopolymerization has been used to create permanent, self-written solid structures in bulk liquid photopolymers [3,4]. The features of this process are similar to the self-writing process described above. The principal difference between photosensitivity and photopolymerization is that in a photopolymer, the index response is delayed by 0.01–1 s relative to the illumination [3,4]. Tapered waveguides have also been written in UV-cured epoxy using a similar, dynamic self-writing process [5]. All these self-writing processes are qualitatively similar.

Here we present an analytical technique developed to study some of the principal features of this class of self-writing processes. We apply this technique to both photosensitivity and photopolymerization, and it can be used to study either the planar or bulk geometry.

We use two partial differential equations to describe self-writing; one to describe light propagation, and another to describe how the refractive index changes in response to light. This model is described in detail in Sec. II. No exact

solutions to this problem are known. The most straightforward approach is to solve these equations numerically, and we have done this for both photosensitivity and photopolymerization using a beam propagation method combined with updates of the refractive index [1,2]. Although this technique provides a detailed and accurate description of the process, it requires intensive use of both computer time and memory. We have also developed a modal decomposition technique [6] for the photosensitivity process where we decompose the electric field and the refractive index into Hermite-Gaussian modes. Although this technique is more efficient than the full simulation, it also only yields purely numerical results. Here we describe an analytical series expansion technique that allows us to describe some important features of self-writing waveguides exactly. In particular, we describe the formation and evolution of maxima in the intensity and index (which we refer to as eyes), which are precursors to waveguide formation.

In previous work, we applied the series expansion technique to a Gaussian beam incident on a planar photosensitive material [1,2]. Here we generalize the technique to both planar and bulk geometries, and to an arbitrary input beam. We

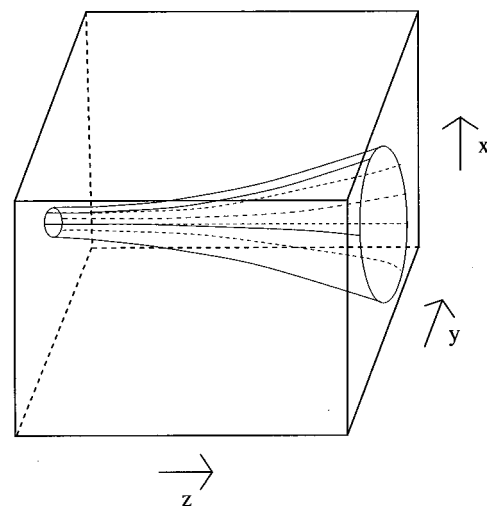


FIG. 1. Schematic of a bulk photosensitive material, showing the initial diffraction of the Gaussian beam.

also take the saturation of the refractive index change and the material loss into account. This allows us to obtain a greater physical insight into the types of waveguides that can be self-written in real photosensitive materials and photopolymers.

Sections II and III describe the model we use to study this self-writing process. In Sec. IV we discuss the maxima that form in the intensity and refractive index (primary eyes), which are precursors to the formation of a waveguide in the material. Section V outlines the way in which series expansions for the intensity and refractive index distributions in the material are calculated, and how they can be used to calculate the trajectories of the primary eyes, and hence calculate the shape of the resulting waveguide. Section VI gives the series expansion results found when the saturation of the refractive index or loss are included in the model. The results of the series technique for photopolymerization are also presented in this section.

## II. MODEL

The paraxial wave equation is used to describe light propagation [7,8]:

$$ik_0n_0\frac{\partial\mathcal{E}}{\partial z} + \frac{1}{2}\nabla_t^2\mathcal{E} + k_0^2n_0\Delta n\mathcal{E} + \frac{i}{2}k_0n_0\alpha\mathcal{E} = 0, \quad (1)$$

where  $k_0$  is the free space wave number,  $n_0$  is the initial refractive index,  $\Delta n(x,y,z,t) = n - n_0$ , where  $n$  is the current refractive index and  $\mathcal{E}(x,y,z,t)$  is the electric field envelope amplitude. We explicitly include a constant loss term in Eq. (1), where  $\alpha$  is the attenuation coefficient. The loss in decibels per unit length is  $4.343\alpha$ . For a planar material,  $\nabla_t^2 = \partial^2/\partial y^2$ , and we assume that the field profile is unaffected in the  $x$  direction [1,2,8]. For a bulk material,  $\nabla_t^2 = \partial^2/\partial x^2 + \partial^2/\partial y^2$ . We have approximated the refractive index term in the paraxial wave equation by a linear factor, because the refractive index changes we consider are small (typically less than 1%) [7].

We use the following simple phenomenological model, which includes saturation effects, to describe the evolution of the refractive index for both photosensitivity and photopolymerization [2–4,9,10]:

$$\frac{\partial\Delta n}{\partial t} = A(\mathcal{E}\mathcal{E}^*)^p \left( 1 - \frac{\Delta n}{\Delta n_s} \right), \quad (2)$$

where  $t$  is the time and  $\Delta n_s$  is the fixed saturation value of the refractive index change. For a photosensitive material,  $\mathcal{E}$  is calculated at time  $t$ . For a photopolymer, the refractive index change due to photopolymerization is delayed by time  $\tau$  (typically 0.01–1 s relative to the illumination) [3]. Hence  $\mathcal{E}$  is calculated at time  $t - \tau$  for a photopolymer [3,4]. For photopolymerization or a one-photon photosensitivity process,  $p=1$ , and for a two-photon photosensitivity process  $p=2$ . The real coefficient  $A$  depends on the material properties, the number of photons ( $p$ ), and the wavelength of the light. As no consensus has been reached on the best model for saturation in a photosensitive material, we choose to use

Eq. (2) because it is simple, and so can give useful analytical results. This model has been previously used to describe photopolymerization [3,4].

In previous work on the planar photosensitive geometry [1,2,6], we ignored the effects of saturation. We did this because the typical maximum refractive index changes required for waveguide formation in the planar geometry are not large. For example, consider a Gaussian beam of width  $20\ \mu\text{m}$  incident on a planar waveguide at the one-photon photosensitivity wavelength of 244 nm. Numerical simulations indicate that a fairly uniform channel waveguide can be written with a maximum refractive index of  $4 \times 10^{-7}$  (at the primary eye in the refractive index), which is so small that the effects of saturation can be ignored. However, for bulk photosensitive materials, we find that the index grows without bound before any waveguiding structure evolves. If saturation is included, we find that by the time a fairly uniform channel waveguide has formed, the maximum refractive index is close to the saturation value. Thus saturation cannot be ignored in bulk geometries.

Many of the results in this paper are based on a Gaussian beam, which is incident from the left on the *input face* ( $z=0$ ). For a planar material

$$\mathcal{E}(y,0,t) = \mathcal{E}_0 \exp(-y^2/a^2), \quad (3)$$

and for a bulk material

$$\mathcal{E}(x,y,0,t) = \mathcal{E}_0 \exp[-(x^2 + y^2)/a^2], \quad (4)$$

where  $a$  is the width of the beam, corresponding to a full width at half maximum (FWHM) of  $\sqrt{2\ln 2}a$  in the intensity.

## III. THE MODEL IN DIMENSIONLESS FORM

Here we minimize the number of independent variables by reducing the equations to a dimensionless form. Because the typical time and length scales in this problem depend on the intensity and the spatial extent of the input profile, we introduce the dimensionless transverse coordinates  $X=x/a$ ,  $Y=y/a$ , where  $a$  is the beam width, as defined in Eqs. (3) and (4). We also define a dimensionless field amplitude  $E = \mathcal{E}/\mathcal{E}_0$ . For non-Gaussian input beams,  $a$  is proportional to some characteristic measure of the transverse spatial extent of the input profile, and  $\mathcal{E}_0$  is a characteristic field amplitude. The paraxial wave equation [Eq. (1)] and the index evolution equation [Eq. (2)] can be made dimensionless using the scalings

$$Z = z/(k_0n_0a^2), \quad (5)$$

$$N = a^2k_0^2n_0\Delta n, \quad (6)$$

$$T = a^2k_0^2n_0A(\mathcal{E}_0\mathcal{E}_0^*)^p t, \quad (7)$$

$$L = a^2k_0n_0\alpha, \quad (8)$$

$$T_d = a^2k_0^2n_0A\mathcal{E}_0\mathcal{E}_0^*\tau \quad (9)$$

$Z$  and  $Y$  are related to the dimensionless distances  $\zeta$  and  $\eta$  used in our previous papers [1,2,6] as follows:  $\zeta = k^2a^2Z$  and  $\eta = kaY$ .

Using these dimensionless quantities, Eqs. (1) and (2) are

$$i\frac{\partial E}{\partial Z} + \frac{1}{2}\nabla^2 E + NE + \frac{iL}{2}E = 0 \quad (10)$$

and

$$\frac{\partial N}{\partial T} = (EE^*)^p \left(1 - \frac{N}{N_s}\right), \quad (11)$$

where in Eq. (11),  $E$  is calculated at time  $T$  for photosensitivity, or at  $T - T_d$  for photopolymerization. Now we take  $\nabla^2 = \partial^2/\partial Y^2$  for the planar geometry, or  $\nabla^2 = \partial^2/\partial X^2 + \partial^2/\partial Y^2$  for the bulk geometry. The Gaussian input profile is

$$E(Y,0,T) = \exp(-Y^2) \quad (12)$$

for the planar geometry or

$$E(X,Y,0,T) = \exp[-(X^2 + Y^2)] \quad (13)$$

for the bulk geometry. In these new dimensionless coordinates, the system of equations formed by Eqs. (10) and (11) along with the initial condition [Eq. (12) or (13)] do not depend on  $a$  or  $\mathcal{E}_0$ , and hence the only remaining parameters in this dimensionless system are  $N_s$ ,  $L$ , and  $T_d$ . This simplification makes our problem much more tractable: for a Gaussian beam, or any beam that can be described by two parameters, we now only have to explore a three-dimensional parameter space, as opposed to a five-dimensional one.

#### IV. PRECURSORS TO WAVEGUIDE FORMATION

Using the numerical simulation described in Sec. I, we have solved Eqs. (10) and (11) using a Gaussian input beam [1]. The major steps in the evolution of a self-written waveguide in a photosensitive material [2] or photopolymer are as follows. The refractive index on axis increases with time and thus the diffraction of the beam decreases. Initially, the waist of the beam is at the input face, and so the intensity has a trivial maximum at the origin. After some time, the refractive index becomes large enough to counteract the diffraction, and this maximum (the *primary eye*) moves away from the input face, along the propagation axis. A similar maximum also forms in the refractive index profile. The locations of these maxima change over time. As this process continues, the waveguide beyond the eye gradually becomes more uniform. Ultimately a channel waveguide is formed in the region beyond the primary eye. For the one-photon photosensitivity process and the photopolymerization process (with reasonable physical values for the delay), a particularly uniform channel waveguide is formed. For more complicated beam shapes, such as beams with multiple maxima in the transverse profile, multiple primary eyes typically form, with one eye corresponding to each transverse maximum.

An eye forms when the refractive index change in the material has become sufficient to overcome the initial diffraction of the beam, and hence the self-written refractive index structure has begun to guide light. Indeed, our numeri-

cal simulations suggest that the eye is always a precursor to the formation of a waveguide at that transverse position in the material. Furthermore, our simulations indicate that the structure of the self-written waveguide is closely related to the trajectories of eyes within the material. Hence we concentrate here on describing the behavior of the primary eyes, and use this information to make predictions about the types of waveguides that can be self-written using photosensitivity or photopolymerization.

In the following discussion, although we refer to eyes in the intensity distribution, the analysis is equally valid for eyes in the refractive index distribution. Also, in the remainder of this section we consider only the planar geometry here. The eye is a local maximum, and so the following conditions must hold at the eye:

$$\frac{\partial I}{\partial Z} = 0, \quad (14)$$

$$\frac{\partial I}{\partial Y} = 0, \quad (15)$$

where  $I = I(Y, Z, T)$  is the intensity. Let  $T = T_0$  be the time at which the eye forms. For  $T < T_0$ , the only maximum that can exist is the trivial one at  $Z = 0$ , and for  $T > T_0$ , there is a maximum somewhere within the material. Hence at time  $T = T_0$ , the following condition must be satisfied:

$$\left(\frac{\partial^2 I}{\partial Z \partial Y}\right)^2 - \frac{\partial^2 I}{\partial Z^2} \frac{\partial^2 I}{\partial Y^2} = 0, \quad (16)$$

so that at the eye position, the local curvature is zero. Given  $I$ , Eqs. (14)–(16) allow us to find the time and position at which the eye forms. Equations (14) and (15) can also be used to find the trajectory of the eye as a function of  $T$ .

We observe from our numerical simulations that eyes are typically located near the input face, at small  $Z$ . Hence we use series expansions for the intensity and the refractive index in the propagation distance,  $Z$ , about the input face ( $Z = 0$ ) to explore the behavior of the eyes. We leave the dependences on time and the transverse coordinates exact in these expansions, and use them to predict the behavior of the eyes.

In Sec. V we describe our method for calculating the series expansions for the intensity and the refractive index in a material that is undergoing a self-writing process.

#### V. SERIES EXPANSION TECHNIQUE

We assume that the refractive index is initially uniform in the plane for the planar waveguide geometry. For a bulk material (Fig. 1), we assume that the refractive index is initially uniform throughout the material. Hence at  $T = 0$ ,  $N = 0$ , and the loss ( $L$ ), is constant and uniform throughout. The input beam profile is taken to be the arbitrary function  $E_0(Y)$  for the planar case, or  $E_0(X, Y)$  for the bulk case.

In calculating these series expansions, we keep the dependences on the transverse coordinates and time exact. We define the normalized intensity to be  $I = EE^*$  and write

$$I = \sum_{q=0}^{\infty} I_q Z^q. \quad (17)$$

Substituting the expansions

$$E = \sum_{q=0}^{\infty} E_q Z^q, \quad (18)$$

$$N = \sum_{q=0}^{\infty} N_q Z^q \quad (19)$$

into the paraxial wave equation, Eq. (10), and the index evolution equation, Eq. (11), recurrence relations can be derived for the coefficients in these series by equating powers of  $Z$ . Note that the coefficients  $E_q$ ,  $I_q$ , and  $N_q$  depend on time and the transverse coordinates. The recurrence relations are

$$E_q = \frac{i}{q} \left( \frac{1}{2} \nabla^2 E_{q-1} + \sum_{k=0}^{q-1} N_k E_{q-1-k} + \frac{iL}{2} E_{q-1} \right) \quad (20)$$

and (for  $p=1$ )

$$N_q = \int_{T_d}^T \frac{I_q(T' - T_d)}{Q(T' - T)} dT' - \frac{1}{N_s} \sum_{k=0}^{q-1} \int_{T_d}^T \frac{N_k(T') I_{q-k}(T' - T_d)}{Q(T' - T)} dT', \quad (21)$$

where  $Q(T) = \exp(-I_0^p T/N_s)$ . The time dependences are given exactly in Eq. (21) and the spatial dependences are suppressed. The recurrence relation for  $p=2$  is obtained by replacing the  $I_r$  in Eq. (21) by  $\sum_{s=0}^r I_s I_{r-s}$ .

Equations (20) and (21) can be used to generate the electric field amplitude and refractive index series expansions for both the photosensitivity and photopolymerization processes. The intensity series expansion is generated using  $I_q = \sum_{k=0}^q E_k E_{q-k}^*$ . The terms in these expansions rapidly become quite complicated for the general case, and we used the mathematical analysis program MATHEMATICA to calculate them.

Some of the first few terms for the photosensitivity process are in the Appendix. Further terms in these expansions have been calculated, but they become increasingly complicated. Later we present some of the higher order terms for special cases. The first few terms for the photopolymerization process are discussed in Sec. VI C.

### A. Investigation of eye trajectories

We find that some quite general and exact results can be obtained for the trajectory of the eyes in the intensity and the refractive index if the series expansions only contain even powers of  $Z$ . In this section we discuss the conditions in which the expansions have this form, and the resulting implications for the eye trajectories.

Equation (A3) shows that the first odd term in the intensity expansion disappears if

$$\text{Im}[E_0^* \nabla^2(E_0)] = LI_0 \quad (22)$$

for all values of the transverse coordinates  $X$  and  $Y$ . The term on the left in Eq. (22) describes the curvature of the incident beam, and the term on the right describes how the

intensity drops off due to loss. For the remainder of this section we consider the planar geometry, and so we can take  $N_s = \infty$ . If we write  $E_0 = r(Y) \exp[i\phi(Y)]$ , Eq. (22) becomes

$$\frac{\partial}{\partial Y} \left( I_0 \frac{\partial \phi}{\partial Y} \right) = LI_0, \quad (23)$$

where  $r^2 = I_0$ . Any physically reasonable  $I_0$  must go to zero as  $Y \rightarrow \pm\infty$ . Hence if we integrate Eq. (23) over all  $Y$ , the right side is a positive constant, and the left side is zero, as long as  $\phi$  is not rapidly varying at  $\pm\infty$ . This indicates that Eq. (23) can only be satisfied for all  $Y$  if  $L=0$ , and hence can only be satisfied if the beam has a flat phase front. Hence if there is loss, or the beam does not have a flat phase front, then the expansions must contain at least one odd term in  $Z$ .

We find that if we take the loss to be zero ( $L=0$ ), and the beam phase front to be flat, then there are no odd terms in the expansions for either the planar or bulk geometries. Hence for simplicity we consider a flat phase front beam in a lossless planar geometry. For a beam with a flat phase front,  $E_0$  can be made real. Then  $I_0 = E_0^2$ , and

$$I_2 = \frac{1}{4} (E_0''^2 - E_0 E_0'''' ) - T (E_0^3 E_0'' - 3E_0^2 E_0'^2) \quad (24)$$

for the  $p=1$  photosensitivity process, where  $E_0'$  is the derivative of  $E_0$  with respect to  $Y$  evaluated at  $Y_0$ .

When there are only even terms in the expansion, Eq. (14) is always satisfied at  $Z=0$ , as there is always either a maximum or a minimum there. Using Eqs (15), (16), and (24), it is straightforward to show that an intensity primary eye forms at time  $T_0$ , which can be found using

$$4E_0^3 E_0'' T_0 = E_0''^2 - E_0 E_0'''' . \quad (25)$$

This is consistent with the earlier result for a Gaussian beam [1]. The right-hand side Eq. (25) is a measure of how strongly the beam diffracts at small  $Z$ . The presence of the fourth derivative indicates that the initial diffraction is very sensitive to the beam profile, because beams that differ only in the fourth derivative of the intensity can diffract at dramatically different rates. This feature is independent of the index evolution. The refractive index change in the input face region acts like a lens on the incident beam. The left-hand side of Eq. (25) is a measure of the strength of this lens. Hence  $T_0$  is the time at which the lens has grown strong enough to counteract the initial diffraction of the beam, and hence form an eye.

We now calculate the initial trajectory of the intensity eye after it has formed. Most primary eyes form at  $Z=0$ , and we consider only this case here. We expand the intensity series expansion about the formation point (i.e.,  $Z = \delta Z$ ,  $Y = Y_0 + \delta Y$  and  $T = T_0 + \delta T$ ). If we assume that  $\delta Z$ ,  $\delta Y$ , and  $\delta T$  are small, this expansion is of the form

$$I \approx a_0 + a_1 \delta Y^2 + a_2 \delta T \delta Z^2 + a_3 \delta Y \delta Z^2 + a_4 \delta Z^4 \quad (26)$$

for  $p=1$ , where the  $a_i$  are constants that depend on the beam profile. Since at the eye there must be a maximum in the  $Y$  direction, we put this expansion into Eq. (15). This leads to

$$2a_1 \delta Y = -a_3 \delta Z^2. \quad (27)$$

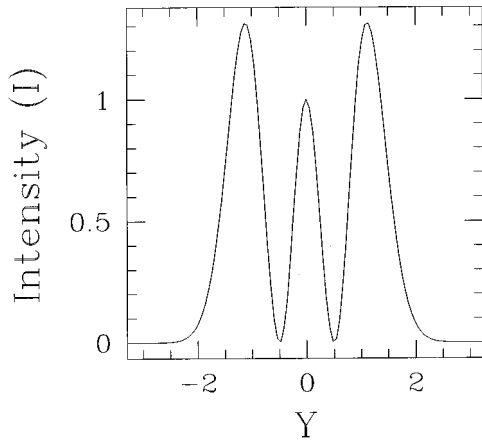


FIG. 2. The intensity in the transverse direction for a second-order Hermite-Gaussian beam [see Eq. (29)].

Hence regardless of the input beam shape, the eye always initially moves away from the input face in a parabolic trajectory. This occurs for both one and two-photon photosensitivity processes. The Gaussian beam is a degenerate example: for this case the trajectory is a straight line along the central axis [2]. In general, any eye that forms on the central symmetry axis of a symmetric beam moves in a straight line along this axis.

At the eye, Eq. (14) must also be satisfied, as the eye is a local maximum, and using this condition we find an equation of the form

$$a_2 \delta T + a_3 \delta Y + 2a_4 \delta Z^2 = 0. \quad (28)$$

Combining Eqs. (27) and (28), we can find the rate at which the eye moves along its parabolic path.

The same analysis can be performed for the trajectory of the refractive index eye. We find the unexpected result that to lowest order the index eye moves along the same trajectory as the intensity eye, but at a different rate. This is true for both one- and two-photon photosensitivity processes. When loss is included, the eye trajectories can be found using the same technique, and we then also find that the intensity and index eyes initially follow the same trajectory, regardless of the loss ( $L$ ).

### 1. Example: second-order Hermite-Gaussian beam

As an example of the application of the series technique we present the analysis of the eye movement for a second-order Hermite-Gaussian profile in a lossless planar structure, without saturation. We choose this particular example because it demonstrates how the structure of quite complicated self-written waveguides can be predicted using the series technique. We consider only the one-photon process here for simplicity. The input beam is of the form

$$E(Y, Z=0, T) = (4Y^2 - 1) \exp(-Y^2), \quad (29)$$

as shown in Fig. 2. This beam has maxima at  $Y_0=0$  and  $Y_0 = \pm \sqrt{5}/2$  (see Fig. 2). For an eye to form, there must be a maximum in the transverse direction, and so in this instance, eyes form at these transverse coordinates. Using Eq. (25), the

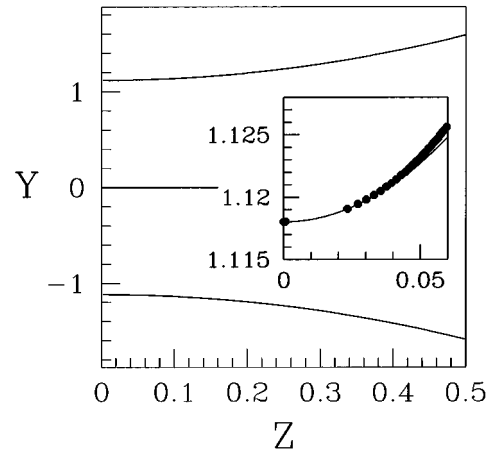


FIG. 3. The initial movement of the primary intensity eyes for a second-order Hermite-Gaussian beam [see Eq. (30)]. The solid lines are the predictions of the series technique, and the dots are results of the full numerical simulation.

eye at  $Y=0$  forms at  $T=1/5=0.2$ , and the eyes at  $Y_0 = \pm \sqrt{5}/2$  form at  $T=e^{2.5}/40 \approx 0.30$ .

The beam is symmetric about  $Y=0$ , and so the eye that forms on this axis remains on axis, as for the Gaussian input beam. The eye that forms at  $Y_0 = \sqrt{5}/2$  initially moves along the path

$$21Z^2 = 5\sqrt{5}(Y - Y_0), \quad (30)$$

which is a special case of Eq. (27), and the eye that forms at  $Y_0 = -\sqrt{5}/2$  follows the mirror image trajectory. The solid lines in Fig. 3 show the way these eyes move just after they form as predicted using this technique. The results of the full numerical simulation agree with these predictions for small  $Z$ , as shown by the dots in the inset in Fig. 3. As expected for a series expansion result, the prediction deviates from the simulation results as  $Z$  becomes larger. As described in Sec. V A, we know that the refractive index eyes follow the same trajectory as the intensity eyes. The eyes are precursors to waveguide formation, and the eye trajectories can be used to predict the resulting structure of the self-written waveguide (see Sec. IV).

Hence our series expansion predicts that three waveguides form; one corresponding to each primary eye. One waveguide forms along the central axis of the material, corresponding to the eye on this axis. As the other two eyes move apart (at least at small  $Z$ ), we predict that the waveguides corresponding to these eyes curve in opposite directions. We have verified this using the full numerical simulation. Figure 4 is a contour plot of the refractive index in the material at a late time in the evolution of the self-written waveguide, and the waveguide indeed is of the form predicted by our analytical results.

For this example we find that we can also use the results of the series technique to estimate the relative depths of these waveguides. If we evaluate the intensity using the series expansion at the eye position just after the eye has formed, we find that for the outer eyes,

$$I(Y_{\text{MAX}}, Z_{\text{MAX}}, T) \approx 1.31 + 0.24 (T - 0.3)^2 \quad (31)$$

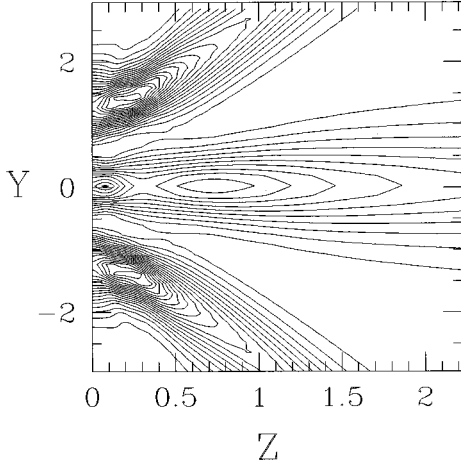


FIG. 4. A contour plot of the refractive index profile, which can be self-written in a planar photosensitive slab using a second-order Hermite-Gaussian beam (see Sec. V A 1).

for  $T > 0.3$ , while for the central eye

$$I(Y_{\text{MAX}}, Z_{\text{MAX}}, T) \approx 1 + 0.09 (T - 0.2)^2 \quad (32)$$

for  $T > 0.2$ . Hence the outer eyes always have a higher intensity than the eye on the central axis. This suggests that the waveguides corresponding to the outer eyes are likely to be more strongly guiding, which is supported by the contours in Fig. 4.

## VI. EFFECT OF OTHER MATERIAL PARAMETERS ON SELF-WRITING PROCESSES

As all materials exhibit some loss and saturation effects, we present here series expansion analysis of these effects on the waveguides that can be self-written in a material. The effect of the time delay of the index response in a photopolymer is also explored using this technique.

### A. Effect of loss in a planar geometry

We consider here the effect of loss in the planar geometry for the one-photon photosensitivity process. We expect that the effect of loss on this self-writing process would be similar for a bulk material. For simplicity, we again take the input beam to be Gaussian [Eq. (12)]. By symmetry, the eye moves along the central axis, so it suffices to consider the expansions on the  $Y=0$  axis. Even though this beam has a flat phase front, there are odd terms in the series expansions for a lossy material [see Eq. (A3)]. This is because to lowest order, the effect of loss is to cause the intensity to drop off linearly with distance into the material. This always occurs, which can be seen by noting that Eq. (A3) does not depend on  $T$ . Hence from Eq. (A3), if a primary eye forms in a lossy material, it cannot form at the origin, and so must form a finite distance into the sample, at  $Z=Z_0$ . We treat the loss ( $L$ ) as a small parameter in order to make this problem tractable: we know that if  $L$  is small, then  $Z_0$  is also small, and so we can ignore higher orders in  $Z_0$ . If there is no loss, then we know that the eye forms at  $T_0=1$  [see Eq. (25)]. Hence

we treat  $T-1$  as a small parameter also. Neglecting small terms, the intensity expansion becomes

$$I \approx 1 - LZ + 2(T-1)Z^2 - 22Z^4. \quad (33)$$

Using Eqs. (14) and (16) for an eye to form gives

$$4(T_0-1)Z_0 - 88Z_0^3 \approx L \quad (34)$$

and

$$(T_0-1) \approx 66Z_0^2. \quad (35)$$

We do not need to use Eq. (15) here because we know by symmetry that the position of the transverse intensity maximum is always  $Y=0$ . Solving Eqs. (34) and (35) simultaneously, the eye forms at time

$$T_0 \approx 1 + \frac{3}{4}(22L^2)^{1/3}. \quad (36)$$

Hence as expected, the presence of loss increases the time taken for the intensity eye to form. The eye forms at position

$$Z_0 \approx \frac{1}{2} \left( \frac{L}{22} \right)^{1/3}. \quad (37)$$

The fractional powers in Eqs. (36) and (37) show that even a small amount of loss dramatically changes the dynamics of this process; the eye forms later, at a finite position in the slab.

When  $L=0$ , there is always a trivial minimum at the origin after the eye forms. For small  $L$ , using Eq. (14), we find the following equation for the position of the eye at time  $T$ , just after it has formed:

$$T - T_0 \approx 22 \left( Z^2 - 3Z_0^2 + 2\frac{Z_0^3}{Z} \right). \quad (38)$$

Equation (38) shows that loss causes two stationary points to form at a finite position within the slab ( $Z=Z_0$ ); one is a maximum and the other a minimum. The position of the minimum moves towards the input face, while the position of the maximum moves away, as it did in the previous results. Hence loss causes the minimum to form at a different position, and change its location over time.

The leftmost dashed line in Fig. 5 shows the eye location as a function of time in the absence of loss. When the loss is 0.5 dB/cm, the movement of the maximum and/or minimum pair is given by the other dashed line. The corresponding simulation results are given by the solid lines in Fig. 5. From this figure, we see that for zero loss, the series expansion agrees very well with the full simulation results for small  $Z$ , as expected. When the loss is taken to be 0.5 dB/cm, the series prediction, although excellent, is not as good as for  $L=0$  (see Fig. 5). This is because in calculating these series results, we have assumed that the loss is a small parameter. For the realistic value of loss chosen here, the agreement is still excellent.

For large values of loss, the minimum becomes deeper. This region reduces the fraction of light guided along the

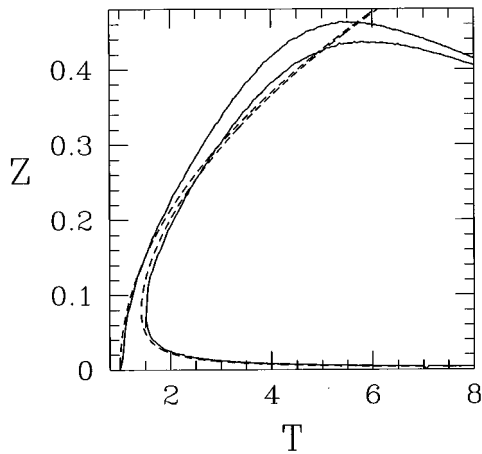


FIG. 5. The left dashed line is the series expansion prediction of the eye movement for zero loss. The right dashed line shows the positions of the maximum and minimum for 0.5dB/cm. The upper part of this curve corresponds to the eye, and the lower part corresponds to the minimum. The solid lines show the corresponding numerical simulation results.

central axis. If the loss is large enough, we find that this effect prevents a channel waveguide from forming along the central axis.

We have also used the series expansion to investigate the effect of loss for the two-photon photosensitivity process, with a Gaussian beam incident on a planar geometry, and we find the same qualitative behavior as for the one-photon process. Equations (36), (37), and (38) all have the same form for the two-photon process; the only difference is in the coefficients.

### B. Effect of saturation

As explained in Sec. II, in a bulk geometry, the saturation of the refractive index needs to be included to avoid the index growing without bound before a waveguide can be self-written in the material. Here we explore the effect of saturation on our self-writing process using a Gaussian beam incident for simplicity. We take the input profile to be of the form in Eq. (13), and we assume that the material is lossless (i.e.,  $L=0$ ). As the material is lossless, and the input profile has a flat phase front, there are no odd terms in the expansion (see Sec. V A). Again, by symmetry, we know that the eye moves along the central axis, so it suffices to consider only the expansions on the  $X=Y=0$  axis.

The intensity series expansion up to the  $I_4$  term is given in the Appendix for both the one- and two-photon processes. Using Eq. (A7), the intensity primary eye forms at time

$$T_0 = \frac{1}{p} \exp(T_0/N_s). \quad (39)$$

Although Eq. (39) cannot be solved exactly for  $T_0$ , it can still be used to obtain some insight. In particular, if  $N_s < e/p$ , Eq. (39) can never be satisfied, and a primary eye can never form. Equation (6) shows that  $N_s$  depends on the physical value of the saturation index ( $\Delta n_s$ ), the diameter of the incident beam, and the wavelength of the light. Hence in a given material, if the beam is too narrow, a self-written

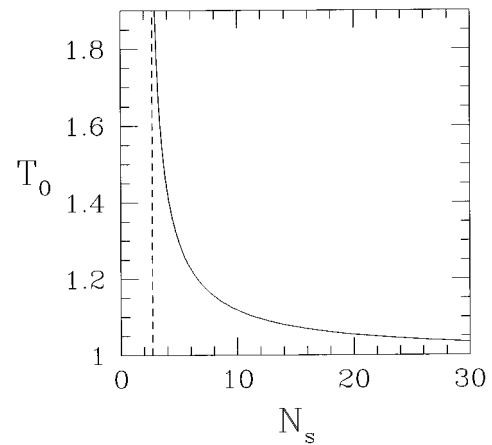


FIG. 6. The formation time of the primary eye ( $T_0$ ) as a function of the refractive index saturation value ( $N_s$ ) for a Gaussian beam in a bulk photosensitive material for  $p=1$ . If  $N_s < e$ , an eye cannot form.  $N_s = e$  is indicated by the dashed vertical line.

waveguide cannot form. Conversely, for a given diameter beam, if  $\Delta n_s$  is too small a waveguide cannot form. We find that for typical beam widths a primary eye, and hence a waveguide, forms in most materials.

Note that as in this case the primary eye forms at  $Z=0$ , the formation time can always be found, regardless of the region of validity of the series. We find that for small  $N_s$  (i.e.,  $N_s \lesssim 5$ ), the range of  $Z$  over which the series expansion results agree with the simulation decreases dramatically. This is probably because the radius of convergence of the series decreases at small  $N_s$ . Hence for small  $N_s$ , even though we can predict whether an eye forms, the series expansions do not provide any useful information about the behavior of the eye after it forms.

The regime where  $N_s$  is small is unlikely to be of interest experimentally, because for typical beam diameters, this range of saturation values is substantially lower than found in real materials. For example,  $N_s=5$  corresponds to  $\Delta n_s \approx 1 \times 10^{-5}$  for a 20  $\mu\text{m}$  beam diameter at  $\lambda=244$  nm, significantly less than typical values of the saturation index [13]. Hence for realistic saturation values the series expansions provide useful information.

Equation (39) predicts that for both one- and two-photon photosensitivity processes  $T_0$  increases as  $N_s$  decreases from infinity, and so it takes longer to form a waveguide with increasing saturation. This is shown for the one-photon case in Fig. 6, which shows  $T_0$  as a function of  $N_s$ , as given by Eq. (39).

We use the method described in Sec. IV to explore the motion of the eye. Because the eye moves along the central axis, and forms at  $Z=0$ , Eq. (16) and Appendix A can be used to show that the trajectory is initially of the form

$$Z = \sqrt{\gamma(T - T_0)}, \quad (40)$$

where  $\gamma$  is the rate at which the eye moves away from the input face. For large  $N_s$  this rate is

$$\gamma \approx \frac{1}{4\sqrt{2}} \left( 1 + \frac{1}{96N_s} \right) \quad (41)$$

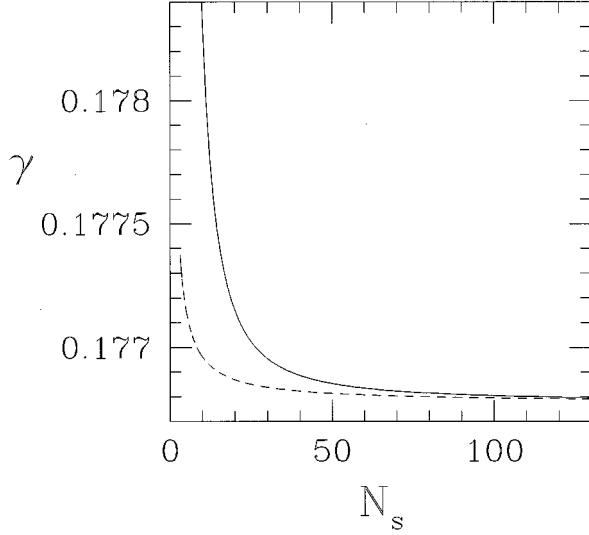


FIG. 7. The solid line gives the rate at which the intensity primary eye moves away from the input face just after it has formed ( $\gamma$ ) [as defined in Eq. (40)] for a Gaussian beam in a bulk material versus  $N_s$  for  $p=1$ . The dashed line gives the first order approximation for large  $N_s$  [Eq. (41)].

for  $p=1$ , where the first order correction due to saturation is included. This correction is shown by the dashed line in Fig. 7. This figure shows that the eye begins to move more quickly as the saturation value of the index decreases from infinity. This trend continues, as is shown by the solid line in Fig. 7, which shows  $\gamma$  as a function of  $N_s$  for  $p=1$ . If the saturation index ( $N_s$ ) is sufficiently large, then it is irrelevant at small times, and so the value of  $N_s$  has little effect on the dynamics; this is demonstrated by the flatness of the curve (Fig. 7) at large  $N_s$ . For the two-photon process the rate is of the same form as Eq. (41), with different coefficients.

### C. Effect of delay on the refractive index response

As discussed in Sec. II, for the photopolymerization process  $p=1$ , and the refractive index response is delayed relative to the illumination. Previous results in this paper correspond to a zero delay. Here we present some results of the series expansion for the intensity for a nonzero delay. Although we have calculated the terms for an arbitrary beam, we present the results for a Gaussian input beam for simplicity. As before, by symmetry we know that the eye remains on the central axis ( $X=Y=0$ ). We find that  $I_0=1$  and

$$I_2=4(T-T_d)Q_d-4, \quad (42)$$

where  $Q_d=\exp[-(T-T_d)/N_s]$ .

As before, an eye forms when Eqs. (14) and (15) are satisfied. Using Eq. (42), this occurs when

$$T_0-T_d=\exp[(T_0-T_d)/N_s]. \quad (43)$$

It is interesting to note that Eq. (43) is the same as for our original one-photon photosensitivity process [Eq. (39)], except that  $T_0$  is replaced by  $T_0-T_d$ . This implies that the time delay simply causes the eye formation time to be de-

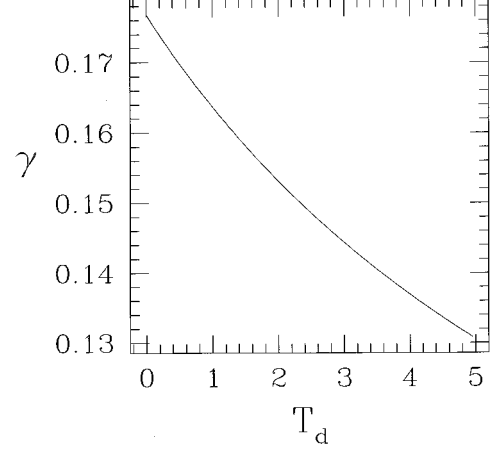


FIG. 8. The rate at which the intensity primary eye moves away from the input face ( $\gamma$ ) for a Gaussian beam in a photopolymer as a function of the delay  $T_d$ .

layed by  $T_d$ . We have found this property is true in general, for an arbitrary incident beam.

The  $I_4$  term in the series expansion is more complicated, and is not shown here. We find that  $I_4$  no longer depends on just  $T-T_d$ . As for the case considered in Sec. VI B, the motion of the eye is again of the form Eq. (40), where  $\gamma$  gives the rate at which the eye initially moves away from the input face. Figure 8 shows  $\gamma$  as a function of the delay  $T_d$ . This figure shows that the eye moves away more slowly as the delay is increased. This is not a large effect;  $\gamma$  changes by less than 30% over the range of  $T_d$  values shown. Hence, to this order, this process is no longer just a delayed replica of the processes we presented earlier. This is not surprising, as in general we would expect differences to occur for different values of  $T_d$ .

In the photopolymerization experiment conducted by Kewitsch and Yariv [3,4], a typical value for the delay is  $\tau=0.1$ s. Their experiment, as shown in Fig. 4 in Ref. [3], takes 30 s, and hence the time delay is not large when compared with the time scale for the self-writing process in this case. Hence we expect that their photopolymerization experiments should be well described by our bulk material model, and so the results for the photosensitive process described throughout this paper should apply here.

## VII. GENERALIZATIONS OF THE SERIES TECHNIQUE

Although the series technique is useful for describing the behavior of the primary eyes while they remain within the radius of convergence of the series, they typically move out of this region. The motivation for the class of techniques we describe here is to extend the validity of the series to larger  $Z$  so that we can explore this self-writing process more fully. However, we show below that the obvious attempts to generalize this problem fail.

One well-known generalization is to use Padé approximants [11]. In particular, if the radius of convergence of a series is limited by a simple pole, then often Padé approximants can be used to remove the singularity, and hence extend the region of validity of the expansion. The  $(N,M)$  Padé approximant is the rational function

$$f_{N,M}(Z) = \frac{\sum_{s=0}^M A_s Z^s}{\sum_{t=0}^N B_t Z^t}, \quad (44)$$

where the  $A_s$  and  $B_t$  are unknown coefficients, and  $Z$  is a complex quantity [11]. The coefficients are found by setting  $f_{N,M}(Z)$  equal to the series in question, and equating coefficients.

We applied this technique to our problem for a number of different  $(N, M)$ . No choice we made gave good quantitative predictions for the behavior of the eye. This can be understood by considering the free propagation form of the electric field amplitude. Assume we have a flat-phase front Gaussian beam, in the planar waveguide geometry. Then the electric field in the slab at  $T=0$ ,  $Y=0$  is

$$E = \frac{1}{\sqrt{1+2iZ}}. \quad (45)$$

If we take  $Z$  to be a complex quantity, then the electric field amplitude has a branch point at  $Z=i/2$  initially. This branch point limits the region of validity of any Padé approximant of the form in Eq. (44).

One established way of coping with singularities of this type is to use the differential Padé generalization [12]. In this generalization, some differential combination of  $E$  is approximated by an expression of the form in Eq. (44). Here Eq. (45) suggests the form

$$\frac{1}{E} \frac{\partial E}{\partial Z} = \frac{\sum_{s=0}^M A_s Z^s}{\sum_{t=0}^N B_t Z^t}. \quad (46)$$

This form removes singularities of the type shown in Eq. (45) exactly. It might be hoped that it would continue to give an improved region of validity at later times also. However, we have proved that even though Eq. (46) can be used to represent the field exactly at  $T=0$ , an infinitesimal time  $dT$  later, the field contains singularities that cannot be expressed by Eq. (46). This explains why these Padé techniques cannot be used here to extend the region of validity of our series expansion results, and it is not clear how Eq. (46) should be generalized to account for these singularities.

## VIII. DISCUSSION AND CONCLUSIONS

We have developed an analytical technique to describe the types of waveguides that can be self-written in photosensitive materials and photopolymers. It should be straightforward to apply this approach to other self-writing processes, as long as the index evolution can be described by a simple model that can then be used to derive the necessary recurrence relations.

As discussed in Sec. II, we use Eq. (2) to model the refractive index evolution because it is the simplest model that is consistent with experiment. Equation (2) has been previously used to model the index evolution, which occurs due to photopolymerization [3,4], and here we also apply it to pho-

tosensitivity. For photosensitivity, some experimental results suggest that the index evolution might be better modeled by a power law [14] but we expect that the results produced by our simpler model should remain valid, except for a scaling in the time parameter [2].

We have shown that in a planar geometry, where the effects of saturation can be ignored, the primary eyes in the intensity and the refractive index initially follow the same (parabolic) path. We have confirmed this using the full numerical simulation, and we find that the paths remain similar for a very long time. This result is surprising, because the refractive index at time  $T$  depends on the entire history of the illumination. Also, although the two eyes follow the same path initially, they travel along these paths at different times. This allows us to make predictions about the resulting self-written waveguide using only the intensity series expansion. This is particularly useful, as the terms in the refractive index expansion take longer to calculate and are often more complex than the corresponding terms in the intensity expansions. This is because the calculation of the coefficient of  $Z^q$  in the index expansion involves the coefficient of  $Z^q$  in the intensity expansion.

As a concrete example of the use of our analytical technique, we investigated the waveguide that forms when a second-order Hermite Gaussian beam is incident on a lossless planar structure. We choose this beam because it has a flat phase front, and so there are no odd terms in the expansions, which makes the analysis easier. Also, the resulting waveguide structure is complicated, and so is a useful test of the series technique. Looking at the behavior of the primary eyes, we predict that three waveguides form, one along the propagation axis, the other two curve outwards. These predictions agree with the results of our full numerical simulation. Without running the full simulation, which is computationally intensive, this technique allows us to determine the structure of the resulting waveguide. Our results for this beam profile suggest that the magnitude of an eye can be used to predict the relative strength of the waveguide which corresponds to that eye. Further work needs to be done to determine how universal this hypothesis is for other beam profiles.

We find that even if we consider flat phase-front beams in a lossless planar geometry, the primary eyes do not always form at the origin. For example, if our input beam is a superposition of two singly peaked beams, then the overlapping tails of these beams can cause a maximum to form at large  $Z$ . We do not consider any such cases here. Also, if the eyes form too far away from the origin, they may lie outside the radius of convergence of the series, and hence cannot be studied with the series expansion technique.

The effect of loss on this self-writing process can also be studied using this analytical technique. We have presented the results for a Gaussian beam in a planar structure. Loss causes a minimum to form along with the primary eye. Even for small values of loss, we have shown that the effect of this minimum is significant. Our analysis only considers the case where the loss is small. We do this for two reasons. As explained in Sec. VI A, if the loss is small, the analysis is more tractable, as we can treat the formation position as a small parameter. Also, the location at which the maximum-minimum pair forms is further inside the material for large loss, and so clearly if the loss is too large, they form outside

the radius of convergence of the series, and cannot be tracked using this technique.

In a bulk material, the effect of saturation needs to be included (see Sec. II), and we find that saturation causes the primary eye to form later, and hence the time taken to form a waveguide is slightly increased. We expect this to be true for other beam profiles also, because saturation slows down the index change, particularly near the saturation index. For the Gaussian beam, we have shown that for very low values of the saturation refractive index, no primary eye can form, and hence no waveguide is self-written in the material. This occurs because the refractive index change can never become large enough to focus in the incident beam. However, for practical values of the saturation index, we find that a primary eye always forms, and leads to the formation of a fairly uniform channel waveguide.

Real materials display both a nonzero loss and a finite refractive index saturation. Although we have studied these effects separately in this paper, we expect that the cumulative effects of these parameters can be inferred from our separate studies. If the loss is not too large, a waveguide still forms. Values of the saturated refractive index tend to be large for both photosensitive materials ( $\Delta n_s = 0.001$ ) [13] and photopolymers ( $\Delta n_s = 0.04$ ) [3,4], and so we expect the saturation to typically increase the time taken to form self-written waveguides slightly. Hence, as the effects of loss and saturation of the index are often small in a real material, we would expect the effects of saturation and loss to combine in a straightforward way. This could be tested using the series technique presented in this paper by keeping both loss and saturation terms in the series expansions.

The region of validity of our series expansions is restricted by poles in the analytic continuation of the electric field amplitude and refractive index at  $Y=0$  to the complex  $Z$  plane. If a generalization of the series technique could be found, which accounted for these singularities, then it would be valid for much larger values of  $Z$ , and thus give improved descriptions of the structure of the waveguides which can be formed.

#### ACKNOWLEDGMENTS

Many of the numerical simulations in this paper were done using the VPP300 supercomputer at the Australian National University Supercomputer Facility. L.P. acknowledges financial support from the Australian Research Council.

#### APPENDIX: TERMS IN THE SERIES EXPANSIONS

The recurrence relations [Eqs (20) and (21)] can be used to generate the coefficients in the series expansions of the intensity and the refractive index for both the photosensitivity and photopolymerization processes. For either the one- or two-photon photosensitivity process, we find

$$I_0 = E_0 E_0^*, \quad (\text{A1})$$

$$N_0 = N_s(1 - Q), \quad (\text{A2})$$

$$I_1 = \text{Im}(E_0 \nabla^2 E_0^*) - LI_0, \quad (\text{A3})$$

$$N_1 = \text{Im}(QTI_0^{p-1} E_0 \nabla^2 E_0^*) - pI_0^p QTL, \quad (\text{A4})$$

$$I_2 = \frac{1}{4} \nabla^2 E_0 \nabla^2 E_0^* - \frac{1}{4} \text{Re}(E_0^* \nabla^4 E_0) - I_1 L - \frac{I_0 L^2}{2} - \frac{pQT I_0^{p-1}}{2} [I_0 \nabla^2 I_0 + p(\nabla I_0)^2 \ln(Qe)], \quad (\text{A5})$$

where  $Q = \exp(-I_0^p T/N_s)$ .

If we consider a Gaussian beam incident on a bulk lossless material, and take  $N_s \neq \infty$ , the intensity series expansion has the following terms. For either photosensitivity process, we find

$$I_0 = 1, \quad (\text{A6})$$

$$I_2 = 4(pTQ - 1). \quad (\text{A7})$$

For the one-photon process, the next term in the expansion is

$$I_4 = 16 - \frac{8QT}{3} \left[ 36 + N_s(1 - Q) - 7T \left( \frac{7}{N_s} + Q \right) + \frac{12T^2}{N_s^2} \right] \quad (\text{A8})$$

and for the two-photon process,

$$I_4 = 16 + \frac{16Q}{3} \left( 2N_s^2(Q - 1) + 2N_s(3Q - 2)T + 5T(4QT - 17) + \frac{170T^2}{N_s} - \frac{48T^3}{N_s^2} \right). \quad (\text{A9})$$

- 
- [1] T. M. Monro, C. M. de Sterke, and L. Poladian, *Opt. Commun.* **119**, 523 (1995).  
 [2] T. M. Monro, C.M. de Sterke, and L. Poladian, *J. Opt. Soc. Am. B* **13**, 2824 (1996).  
 [3] A. S. Kewitsch and A. Yariv, *Opt. Lett.* **21**, 24 (1996).  
 [4] A. S. Kewitsch and A. Yariv, *Appl. Phys. Lett.* **68**, 455 (1996).  
 [5] S. J. Frisken, *Opt. Lett.* **18**, 1035 (1993).  
 [6] T. M. Monro, L. Poladian, and C. M. de Sterke, *J. Opt. Soc. Am. A* **14**, 2180 (1997).  
 [7] A. E. Siegman, *Lasers* (University Science Books, Mill Valley, 1986), Chap. 16.  
 [8] C. M. de Sterke and J. E. Sipe, *J. Opt. Soc. Am. A* **7**, 636 (1990).  
 [9] V. Mizrahi, S. LaRochelle, G. I. Stegeman, and J. E. Sipe, *Phys. Rev. A* **43**, 433 (1991).  
 [10] C. M. de Sterke, S. An, and J. E. Sipe, *Opt. Commun.* **83**, 315 (1991).  
 [11] P. R. Graves-Morris, *Padé Approximants* (The Institute of Physics, London, 1973), Chap. 1.  
 [12] M. E. Fisher, *Reports on Progress in Physics*, Vol XXX (II) (The Institute of Physics, London, 1967), Chap. 6.  
 [13] T. Erdogan, V. Mizrahi, P. J. Lemaire, and D. Monroe, *J. Appl. Phys.* **76**, 73 (1994).  
 [14] D. A. Anderson, V. Mizrahi, T. Erdogan, and A. E. White, *Electron. Lett.* **29**, 566 (1993).